Inorg. Chem. **2006**, *45*, 3878–3886

Toward a More General Synthetic Route to Paramagnetic Solids Containing $RCNSSS^{\bullet+}$ Radical Cations. A Structure–Property Correlation for $RCNSSS^{\bullet+}$ ($R = F_5C_2$, Cl_3C)

Andreas Decken,[†] Saba M. Mattar,[†,‡] Jack Passmore,*[,†] Konstantin V. Shuvaev,[†] and Laurence K. Thompson[§]

Department of Chemistry, University of New Brunswick, Fredericton E3B 6E2, Canada, Centre for Laser, Atomic and Molecular Sciences, University of New Brunswick, Fredericton E3B 6E2, Canada, and Department of Chemistry, Memorial University of Newfoundland, St. John's A1B 3X7, Canada

Received April 14, 2005

Reaction of Cl_3CN and F_5C_2CN with a 1:1 mixture of $S_4(AsF_6)_2$ and $S_8(AsF_6)_2$ affords the paramagnetic solids $Cl_3CNSSSAsF_6$ (**$1CCl_3AsF_6$**) and $F_5C_2CNSSSAsF_6$ (**$1C_2F_5AsF_6$**). Isotropic electron paramagnetic resonance spectra of **$1CCl_3AsF_6$** and **$1C_2F_5AsF_6$** in SO_2 consist of a single line with $g = 2.01675$ and 2.01580, respectively. The structure of **$1CCl_3AsF_6$** contains chains of radical cations with relatively close interchain interactions. In contrast, chains are isolated in **$1C_2F_5AsF_6$**. The magnetic behavior of both compounds was interpreted as that of 1D Heisenberg antiferromagnetic chains (**$1CCl_3AsF_6$**, $J = -34$ cm^{-1}, $\theta = -9$ cm^{-1}, TIP = 0.00082, $\rho = 0.012$; **$1C_2F_5AsF_6$**, $J = -21$ cm^{-1}, $\theta = -4.2$ cm^{-1}, TIP = 0.00092, $\rho = 0.065$). Density functional theory calculated and experimental magnetic coupling constants were in good agreement. The correlation between intermolecular S···S contacts and the strength of magnetic couplings was established.

Introduction

Over the past 2 decades, there has been much effort in exploring and understanding the unusual physical, conducting, and magnetic properties of stable 7π thiazyl radicals, e.g., RCNSSN,[1] RCSNSCR′,[2] RCNSNS,[3] RCSSNCR′,[2a,4] and recently structurally characterized RCNC(R′)NSCR″[5] (Chart 1). On the other hand, the radical cations $RCNSSS^{\bullet+}$, formally derived from $RCNSSN^{\bullet}$ and $RCNSNS^{\bullet}$ by isoelectronic substitution of $N^{\bullet}$ for S^{+}, have hardly been explored. This ring system was discovered in an attempt to "trap" $S_3^{\bullet+}$ by CF_3CN in a SO_2 solution of $S_4(AsF_6)_2$ and $S_8(AsF_6)_2$[6a] (Scheme 1). This was, in fact, successful, and CF_3-

Chart 1

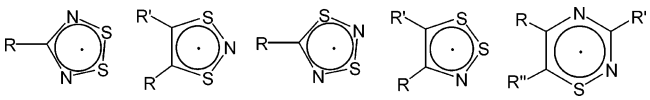

* To whom correspondence should be addressed. E-mail: passmore@unb.ca.

† Department of Chemistry, University of New Brunswick.

‡ Centre for Laser, Atomic and Molecular Sciences, University of New Brunswick.

§ Memorial University of Newfoundland.

(1) (a) Rawson, J. M.; Banister, A. J.; Lavender, I. *Adv. Heterocycl. Chem.* **1995**, *62*, 137. (b) Oakley, R. T. *Adv. Mater.* **1994**, *6*, 798. (c) Rawson, J. M.; Palacio, F. *Struct. Bonding* **2001**, *100*, 93. (d) Alberola, A.; Less, R. J.; Pask, C. M.; Rawson, J. M.; Palacio, F.; Oliete, P.; Paulsen, C.; Yamaguchi, A.; Farley, R. D.; Murphy, D. M. *Angew. Chem., Int. Ed.* **2003**, *42*, 4782. (e) Banister, A. J.; Bricklebank, N.; Lavender, I.; Rawson, J. M.; Gregory, C. I.; Tanner, B. K.; Clegg, W.; Elsegood, M. R. J.; Palacio, F. *Angew. Chem., Int. Ed. Engl.* **1996**, *35*, 2533. (f) Alberola, A.; Less, R. J.; Palacio, F.; Pask, C. M.; Rawson, J. M. *Molecules* **2004**, 771. (g) Alberola, A.; Clarke, C. S.; Haynes, D. A.; Pascu, S. I.; Rawson, J. M. *J. Chem. Soc., Chem. Commun.* **2005**, 4726. (h) Rawson, J. M.; Luzon, J.; Palacio, F. *Coord. Chem. Rev.* **2005**, 2631.

(2) (a) Rawson, J. M.; McManus, G. D. *Coord. Chem. Rev.* **1999**, *189*, 135. (b) Fujita, W.; Awaga, K.; Takahashi, M.; Takeda, M.; Yamazaki, T. *Chem. Phys. Lett.* **2002**, *362*, 97. (c) Fujita, W.; Awaga, K. *Science* **1999**, *286*, 261. (d) Du, H.; Haddon, R. C.; Krossing, I.; Passmore, J.; Rawson, J. M.; Schriver, M. J. *J. Chem. Soc., Chem. Commun.* **2002**, 1836. (e) Parsons, S.; Passmore, J. *Acc. Chem. Res.* **1994**, *27*, 101. (f) Brownridge, S.; Haddon, R. C.; Oberhammer, H.; Parsons, S.; Passmore, J.; Schriver, M. J.; Sutcliffe, L.; Westwood, N. P. C. *J. Chem. Soc., Dalton Trans.* **2000**, 3365. (g) Brusso, J. L.; Clements, O. P.; Haddon, R. C.; Itkis, M. E.; Leitch, A. A.; Oakley, R. T.; Reed, R. W.; Richardson, J. F. *J. Am. Chem. Soc.* **2004**, *126*, 8256.

(3) (a) Antorrena, G.; Brownridge, S.; Cameron, T. S.; Palacio, F.; Parsons, S.; Passmore, J.; Thompson, L. K.; Zarlaida, F. *Can. J. Chem.* **2002**, *80*, 1568. (b) Passmore, J.; Sun, X.; Parsons, S. *Can. J. Chem.* **1992**, *70*, 2972. (c) Burford, N.; Passmore, J.; Schriver, M. J. *J. Chem. Soc., Chem. Commun.* **1986**, 140. (d) Passmore, J.; Sun, X. *Inorg. Chem.* **1996**, *35*, 1313. (e) Cameron, T. S.; Lemaire, M. T.; Passmore, J.; Rawson, J. M.; Shuvaev, K. V.; Thompson, L. K. *Inorg. Chem.* **2005**, *44*, 2576.

10.1021/ic050577n CCC: $33.50
Published on Web 04/12/2006

Scheme 1

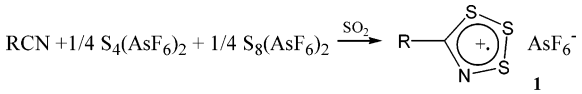

$(CNSSS^{+\cdot})_2(AsF_6^-)_2$ R = CF_3, **1CF$_3$AsF$_6$**; R = CCl_3, **1CCl$_3$AsF$_6$**; R = C_2F_5, **1C$_2$F$_5$AsF$_6$**

2

$CNSSSAsF_6$ (**1CF$_3$AsF$_6$**), a stable paramagnetic solid, was prepared in high yield. Later isolated $(CNSSS)_2^{\bullet\bullet 2+}$ (**2**) was the only sterically unhindered, nonmetal diradical other than O_2 to retain its paramagnetism in all states.[6b,c] Thus, utilization of radical cations **1** as building blocks for materials with unique magnetic properties is an effective potential strategy in suppressing the ubiquitous Peierls distortion, to which the vast majority of neutral thiazyl radicals are prone, although there are some exceptions.[1,4d,5c] Consequently, the preparation of new derivatives of **1** and establishment of a correlation between their structural and magnetic properties are of importance in determining their potential as precursors to novel magnetic materials. Below we report the preparation and isolation of two new derivatives of a rare $RCNSSS^{\bullet+}$ radical cation and show that they maintain their paramagnetism in the solid state.

Experimental Section

Materials. C_2F_5CN (no purity listed; PCR Research Chemicals, Inc., Gainsville, FL) and CCl_3CN (98%, Aldrich, Madison, WI) were used as received. The mixture of $S_4(AsF_6)_2$ and $S_8(AsF_6)_2$ (1:1 ratio) was prepared by condensing AsF_5 and traces of Br_2 onto S_8 (vacuum-dried) in the appropriate mole ratio in liquid SO_2. SO_2 (liquid air, 99.9998%) and freon-11 ($CFCl_3$) were distilled onto CaH_2 and stored for at least 24 h prior to use.

General Procedures. All reactions were performed in two-bulb, two-valve Pyrex vessels incorporating 25-mL bulbs using techniques that have been described previously.[7] Solid reagents and crystals were manipulated on Vacuum Atmospheres Dri-Lab equipment with a Dri-Train (HE-493) and 1 kg of 3-Å molecular sieves contained in an internal circulating drying unit. Fourier transform infrared (FT-IR) spectra of Nujol mulls between KBr disks were recorded on a Thermo Nicolet FT-IR 470 spectrometer (32 scans; resolution, 2.0 cm^{-1}). FT-Raman spectra were recorded at 293 K on a Bruker IFS66 FT-IR spectrometer equipped with a Bruker FRA106 FT-Raman accessory using a Nd:YAG laser (emission wavelength, 1064 nm; maximum laser power, 3009 mW; used laser power, 5.5%). Samples were sealed in melting point capillaries, and data were collected in the backscattering mode (180° excitation; resolution, 2.0 cm^{-1}). Electron paramagnetic resonance (EPR) spectra were recorded with modified Varian E3 and E104 spectrometers. The microwave frequencies were measured with an EIP 371 frequency counter, and the magnetic field was calibrated with a solid sample of diphenylpicrylhydrazyl ($g = 2.0036$) and a Bell 640 gaussmeter. Samples were placed in 4-mm (o.d.) quartz tubes. Variable-temperature magnetic susceptibility data were obtained using a SQUID magnetometer employing a magnetic field of 10 000 Oe. Pressed-pellet conductivity measurements were carried out at the University of Waterloo, Ontario, Canada, using the apparatus described in ref 8a. Elemental analyses were obtained from Galbraith Laboratories, Inc., Knoxville, TN.

Theoretical Calculations. The molecular geometry optimizations and vibrational frequency calculations were performed at the MPW1PW91[8b] level of theory employing the 6-31G(d) and 6-311G+(2df) basis sets using the *Gaussian 03* suite of programs[8c] and visualized by *MOLEKEL*.[8d] The optimized geometries were minima as indicated by the absence of imaginary frequencies. Vibrational frequencies were animated and assigned using *MOLEKEL*.[8d] Natural bond order (NBO) charges were calculated from the optimized geometry at the MPW1PW91/6-311+G(2df) level of theory.

Fitted (experimental) magnetic exchange coupling constants (J) are from the Hamiltonian $H = -2JS_1 \cdot S_2$. Negative and positive J values imply antiferromagnetic and ferromagnetic interaction, respectively. Calculated J values were obtained from the following formula:[8e] $(E_{BS} - E_{HS})/(\langle S\rangle_{HS}^2 - \langle S\rangle_{BS}^2)$, with the geometries of radical-pairs taken from X-ray structures. Single-point energy calculation of the broken symmetry state[8f] was carried out on UB3LYP/PBE0PBE/MPW1PW91/6-31G* levels of theory (keyword *guess = mix*), with fine integration grids and tight self-consistent-field calculation criteria.

Preparation of Compound 1CCl$_3$AsF$_6$. Cl_3CCN (0.3745 g, 0.002 592 mol) in 13.36 g of SO_2 was poured onto a solid (0.8203 g, 0.000 719 5 mol, 11% excess) 1:1 mixture of $S_4(AsF_6)_2$ and $S_8(AsF_6)_2$ ("S_3AsF_6") in 5 aliquots during 3 h with stirring. The mass

(4) (a) Beer, L.; Brusso, J. L.; Cordes, A. W.; Haddon, R. C.; Itkis, M. E.; Kirschbaum, K.; MacGregor, D. S.; Oakley, R. T.; Pinkerton, A. A.; Reed, R. W. *J. Am. Chem. Soc.* **2002**, *124*, 9498. (b) Beer, L.; Britten, J. F.; Brusso, J. L.; Cordes, A. W.; Haddon, R. C.; Itkis, M. E.; MacGregor, D. S.; Oakley, R. T.; Reed, R. W.; Robertson, C. M. *J. Am. Chem. Soc.* **2003**, *125*, 14394. (c) Beer, L.; Brusso, J. L.; Cordes, A. W.; Haddon, R. C.; Itkis, M. E.; Kirschbaum, K.; MacGregor, D. S.; Oakley, R. T.; Pinkerton, A. A.; Reed, R. W. *J. Am. Chem. Soc.* **2002**, *124*, 9498. (d) Beer, L.; Cordes, A. W.; Haddon, R. C.; Itkis, M. E.; Oakley, R. T.; Reed, R. W.; Robertson, C. M. *J. Chem. Soc., Chem. Commun.* **2002**, 1872. (e) Cordes, A. W.; Haddon, R. C.; Oakley, R. T. *Phosphorus, Sulfur Silicon Relat. Elem.* **2004**, *179*, 673.

(5) (a) Kaszynski, P. *Molecules* **2004**, *9*, 716. (b) Zienkiewicz, J.; Kaszynski, P.; Young, V. G. *J. Org. Chem.* **2004**, *69*, 7525. (c) Beer, L.; Haddon, R. C.; Itkis, M. E.; Leitch, A. A.; Oakley, R. T.; Reed, R. W.; Richardson, J. F.; VanderVeer, D. G. *J. Chem. Soc., Chem. Commun.* **2005**, 1218.

(6) (a) Cameron, T. S.; Haddon, R. C.; Mattar, S. M.; Parsons, S.; Passmore, J.; Ramirez, A. P. *Inorg. Chem.* **1992**, *31*, 2274. (b) Boyle, P. D.; Parsons, S.; Passmore, J.; Wood, D. J. *J. Chem. Soc., Chem. Commun.* **1993**, 199. (c) Enright, G. D.; Morton, J. R.; Passmore, J.; Preston, K. F.; Thompson, R. C.; Wood, D. J. *J. Chem. Soc., Chem. Commun.* **1996**, 967.

(7) Murchie, M. P.; Kapoor, R.; Passmore, J.; Schatte, G. *Inorg. Synth.* **1996**, *31*, 80.

(8) (a) Wudl, F.; Bryce, M. R. *J. Chem. Educ.* **1990**, *67*, 714. (b) Adamo, C.; Barone, V. *J. Chem. Phys.* **1998**, *108*, 664. (c) Frisch, M. J.; Trucks, G. W.; Schlegel, H. B.; Scuseria, G. E.; Robb, M. A.; Cheeseman, J. R.; Montgomery, J. A., Jr.; Vreven, T.; Kudin, K. N.; Burant, J. C.; Millam, J. M.; Iyengar, S. S.; Tomasi, J.; Barone, V.; Mennucci, B.; Cossi, M.; Scalmani, G.; Rega, N.; Petersson, G. A.; Nakatsuji, H.; Hada, M.; Ehara, M.; Toyota, K.; Fukuda, R.; Hasegawa, J.; Ishida, M.; Nakajima, T.; Honda, Y.; Kitao, O.; Nakai, H.; Klene, M.; Li, X.; Knox, J. E.; Hratchian, H. P.; Cross, J. B.; Bakken, V.; Adamo, C.; Jaramillo, J.; Gomperts, R.; Stratmann, R. E.; Yazyev, O.; Austin, A. J.; Cammi, R.; Pomelli, C.; Ochterski, J. W.; Ayala, P. Y.; Morokuma, K.; Voth, G. A.; Salvador, P.; Dannenberg, J. J.; Zakrzewski, V. G.; Dapprich, S.; Daniels, A. D.; Strain, M. C.; Farkas, O.; Malick, D. K.; Rabuck, A. D.; Raghavachari, K.; Foresman, J. B.; Ortiz, J. V.; Cui, Q.; Baboul, A. G.; Clifford, S.; Cioslowski, J.; Stefanov, B. B.; Liu, G.; Liashenko, A.; Piskorz, P.; Komaromi, I.; Martin, R. L.; Fox, D. J.; Keith, T.; Al-Laham, M. A.; Peng, C. Y.; Nanayakkara, A.; Challacombe, M.; Gill, P. M. W.; Johnson, B.; Chen, W.; Wong, M. W.; Gonzalez, C.; Pople, J. A.; *Gaussian 03*, revision C.02; Gaussian, Inc.: Wallingford, CT, 2004. (d) Flükiger, P.; Lüthi, H. P.; Portmann, S.; Weber, J. *MOLEKEL 4.3*; Swiss Center for Scientic Computing, Manno, Switzerland, 2000−2002. (e) Nagao, H.; Nishino, M.; Shigeta, Y.; Soda, T.; Kitagawa, Y.; Onishi, T.; Yoshioka, Y.; Yamaguchi, K. *Coord. Chem. Rev.* **2000**, *198*, 265. (f) Noodleman, L.; Norman, J. G. *J. Chem. Phys.* **1979**, *70*, 4903. Noodleman, L. *J. Chem. Phys.* **1981**, *74*, 5737.

Table 1. Experimental and Calculated [MPW1PW91/6-311+G(2df)] Vibrational Frequencies and Intensities for **1CCl$_3$AsF$_6$** and **1C$_2$F$_5$AsF$_6$**

$Cl_3CCNSSSAsF_6$, **1CCl$_3$AsF$_6$**				$F_5C_2CNSSSAsF_6$, **1C$_2$F$_5$AsF$_6$**			
IR	Raman[a]	calcd (IR, Raman)	assignment[b]	IR	Raman	calcd (IR, Raman)	assignment
1528w	1528(9)	1602 (20, 42)	ν_s(C−N)	1552w		1627 (3, 15)	ν_s(C−N)
1508vw	1510(4)		?	1333vs		1340 (287, 7)	ν_s(C(6)−C(12))
				1260vs		1295 (114, 7)	ν(C_2F_5)
				1230vs		1252 (70, 1)	ν(C_2F_5)
800s		820 (118, 11)	ν(CCl_3)	1213vs		1250 (262, 5)	ν(C_2F_5)
1083m	1081(4)	1104 (9, 10)	ν_s(C−C)	1179vs		1201 (164, 4)	ν_s(C(1)−C(6))
				1104m			?
787s	786(3)	803 (112, 5)	ν(CCl_3)	1079vs		1107 (124, 4)	ν(C_2F_5)
897ms		920 (27, 3)	ν_s(S−N)	889s		898 (13, <1)	ν_s(S−N)
overl.		745 (47, 1)	ν_{as}(C−C)	850mw		885 (72, 2)	ν_{as}(C(1)−C(6))
				814w			?
				744s	742	754 (60, 7)	ν_{as}(C(1)−C(6)) + ν(C_2F_5)
700vs	705(5)		ν_3(AsF_6^-)	700vs	700		ν_3(AsF_6^-)
673s	673(21)		ν_1(AsF_6^-)	674vs	674		ν_1(AsF_6^-)
						686 (2, 5)	ν(C(1)−C(6)) oop
622m	621(20)	634 (7, 14)	δ(NCS(3)) i.p.	639m	639	648 (12, 8)	δ(NCS(3)) ip
557m	560(3)		ν_2(AsF_6^-)	567mw			ν_2(AsF_6^-)
						598 (2, 2)	
570m		597 (7, <1)	δ(CN) oop	531mw		559 (8, <1)	δ(CN) oop
532w	532(45)	522 (6, 62)	ν(S_2−S_3)	502vw	500	547 (<1, 19)	ν(S_2−S_3)
				540mw	538	537 (10, <1)	δ(CN) + ν(C_2F_5)
	453(15)	435 (1, 13)	ring twist ip			461 (<1, <1)	ring deform ip
	472(22)	446 (6, 12)	ν(S_1−S_2)	449mw	472	438 (6, 13)	ν(S_1−S_2)
	424(28)	387 (<1, 7)	ring twist ip			410 (3, 7)	ring twist ip
	378(11)	336 (<1, 2)	ring deform ip			365 (<1, 1)	ring deform ip
396vs			ν_4(AsF_6^-)			335 (<1, 1)	ring twist ip
	333(4)	318 (<1,<1)	δ(SN) oop			314 (1, <1)	δ(SN) oop
	238(9)	243 (<1, 2)	ring deform oop			260 (<1, 3)	ring breath
		237 (2, 2)	ring breath			225 (5, 1)	ring def oop
	217(38)	207 (11, 2)	ring breath			213 (1, <1)	ring def oop
						150 (3, <1)	ring twist ip
	152(30)	143 (<1, <1)	ring def oop			128 (<1, <1)	δ(S_1−S_2) oop
	117(25)	97 (0, 3)	ring bent			74 (<1, 1)	ring bent
						53 (<1, <1)	ν(C_2F_5) twist
		9 (0, 3)	ring twist oop			26 (<1, 3)	ring twist oop

[a] Intensities are given as peak heights. [b] Atom labeling given in Figure 1.

of SO_2 was slowly reduced to about 1 g while holding the second bulb at 0 °C, after which the soluble portion was carefully poured into the second bulb and the volatiles were removed by evacuation. A total of 0.60 g (46% yield based on Cl_3CCN) of red-brown crystalline **1CCl$_3$AsF$_6$** was collected in a drybox. Elem anal. Found/calcd (%): C, 5.52/5.59; N, 3.10/3.26. Experimental and calculated IR and Raman frequencies of **1CCl$_3$AsF$_6$** are listed in Table 1. The IR spectrum of the soluble brown portion was identical with that of pure **1CCl$_3$AsF$_6$**. The soluble fraction (0.49 g) was recrystallized from a 10:1 (volume ratio) freon-11/SO_2 mixture, recovering an additional 0.256 g of crystalline **1CCl$_3$AsF$_6$** and thus increasing the yield to 77%.

Preparation of Compound 1C$_2$F$_5$AsF$_6$. F_5C_2CCN (0.368 g, 0.002 54 mol) in 11.23 g of SO_2 was poured onto a solid (0.721 g, 0.000 632 4 mol) 1:1 mixture of $S_4(AsF_6)_2$ and $S_8(AsF_6)_2$ ("S_3AsF_6"). The system was allowed to react for 3 days. The volatiles were removed, and the residue was recrystallized from a 2:1 (volume ratio) freon-11/SO_2 mixture. A total of 0.892 g (82% based on F_5C_2CCN) of red-orange crystalline **1C$_2$F$_5$AsF$_6$** was collected in a drybox. Elem anal. Found/calcd (%): C, 7.82/8.38; N, 3.06/3.26. Experimental and calculated IR and Raman frequencies of **1C$_2$F$_5$AsF$_6$** are listed in Table 1.

Other related preparations of **1CCl$_3$AsF$_6$** and **1C$_2$F$_5$AsF$_6$** are listed in Table S1 in the Supporting Information.

X-ray Crystal Structure Determination. Crystals of **1CCl$_3$AsF$_6$** and **1C$_2$F$_5$AsF$_6$** were grown from liquid SO_2 by slow evaporation of the solvent with a temperature gradient of 5 °C (+5 to 0 °C). Crystal data for **1CCl$_3$AsF$_6$**: $C_2AsCl_3F_6NS_3$, M = 429.48, cryst dimens 0.1 × 0.2 × 0.35 mm, red-brown needle, orthorhombic, space group *Pbca*, a = 8.7769(9) Å, b = 11.8319(11) Å, c = 22.826(2) Å, $\alpha = \beta = \gamma = 90°$, V = 2370.4(4) Å^3, T = 198(2) K, Z = 8, 15 389 reflections collected, 2706 independent reflections (R_{int} = 0.0276), R1 = 0.0271, wR2 = 0.0661 refined on F^2. Crystal data for **1C$_2$F$_5$AsF$_6$**: $C_3AsF_{11}NS_3$, M = 430.14, cryst dimens 0.50 × 0.45 × 0.20 mm, red-orange plate, monoclinic, space group $P2_1/c$, a = 15.112(3) Å, b = 5.8204(12) Å, c = 14.503(3) Å, $\alpha = \gamma = 90°$, β = 112.439(3)°, V = 1179.1(4) Å^3, T = 198(1) K, Z = 4, 5594 reflections collected, 2044 independent reflections (R_{int} = 0.0490), R1 = 0.0591, wR2 = 0.2205 refined on F^2. All measurements were made on a Bruker AXS P4/SMART 1000 diffractometer with graphite-monochromated Mo Kα radiation [μ(Mo Kα) = 14.32 cm^{-1}]. The structure was solved by direct methods (*SHELX97*: Sheldrick, G. M., 1997), and all atoms were refined anisotropically.

Results and Discussion

Previously, we found that a serious impediment to the generality of the $S_4(AsF_6)_2/S_8(AsF_6)_2$ and the RCN route to the $RCNSSSAsF_6$ salts was that other products were formed with RCN of low ionization potentials (IPs; e.g., C_6F_5CN, 10.1 eV;[9a] CH_3CN, 12.2 eV[9b,c]). It was proposed that IPs of greater than ca. 13 eV were required for the synthesis of salts of **1**[9a] (e.g., IP[CF_3CN], 13.9 eV; IP[$(CN)_2$], 13.4 eV). However, there was evidence that **1** was produced as an intermediate,[9a] and therefore we attempted to adopt a

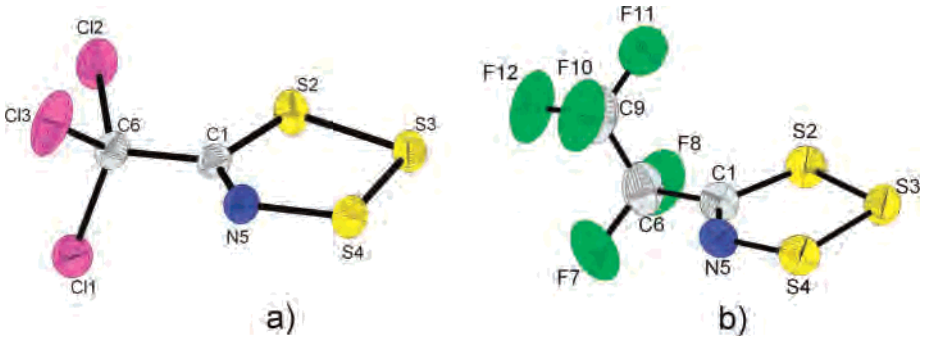

Figure 1. Diamond depiction of $\mathbf{1CCl_3}^{\bullet+}$ (a) and $\mathbf{1C_2F_5}^{\bullet+}$ (b). The internal parameters are listed in Table 2. Thermal ellipsoids are drawn at 50% probability. The numbering scheme for $\mathbf{1C_2F_5}^{\bullet+}$ was changed for the sake of uniform comparison of intramolecular dimensions with the other compounds.

Table 2. Experimental (X-ray) and Calculated [MPW1PW91/6-311+G(2df)] Bond Distances and Angles of $\mathbf{1CF_3}^{\bullet+}$, $\mathbf{1CCl_3}^{\bullet+}$, $\mathbf{1C_2F_5}^{\bullet+}$, and **2**

	$X_3CNSSS^{\bullet+}$, X = Cl, $\mathbf{1CCl_3}^{\bullet+}$		$X_5C_2CNSSS^{\bullet+}$, X = F, $\mathbf{1C_2F_5}^{\bullet+}$		$X_3CCNSSS^{\bullet+}$, X = F, $\mathbf{1CF_3}^{\bullet+}$	$(CNSSS)_2(AsF_6)_2$, **2**
	X-ray	calcd	X-ray	calcd	X-ray	X-ray
			Bond Distances, Å			
C1−N5	1.272(3)	1.270	1.289(13)	1.269	1.259(11)	1.284(3)
C1−S2	1.751(3)	1.754	1.740(11)	1.754	1.717(9)	1.748(3)
N5−S4	1.611(2)	1.595	1.594(9)	1.597	1.652(8)	1.600(2)
S2−S3	2.0164(10)	2.039	2.008(4)	2.025	1.998(4)	2.018(1)
S3−S4	2.0695(10)	2.092	2.068(4)	2.100	2.056(4)	2.070(1)
C1−C6	1.523(3)	1.526	1.515(15)	1.532	1.547(12)	1.462(5)
C6−X1[a]	1.760(3)	1.755	1.333(16)	1.323	1.321(13)	
C6−X2	1.762(3)	1.777	1.320(14)	1.340	1.333(11)	
C6−X3	1.743(3)	1.755	1.52(2)	1.557	1.332(14)	
C9−F10			1.302(16)	1.320		
C9−F11			1.325(18)	1.330		
C9−F12			1.321(14)	1.309		
S2···X2	2.925(1)	2.850	2.819(9)	2.732	2.746(7)	
			Selected Bond Angles, deg			
C6−C1−S2	116.71(18)	116.1	116.5(8)	115.8	116.0(6)	116.6(2)
C1−S2−S3	97.66(9)	97.5	97.5(3)	97.7	97.1(3)	96.83(9)
S2−S3−S4	97.00(4)	96.5	97.04(15)	96.6	97.49(15)	97.52(4)
S3−S4−N5	101.17(9)	100.5	101.7(3)	100.4	101.2(3)	101.02(9)
C1−N5−S4	121.59(19)	123.6	120.7(7)	123.2	117.9(6)	121.3(2)
C6−C1−N5	120.7(2)	122.0	120.4(10)	122.0	117.7(8)	120.3(2)
			Selected Dihedral Angles, deg			
X2-C6−C1−S2	−16.37(24)	0.00	25.94(13)	11.9	−1.81(11)	

[a] In $\mathbf{1C_2F_5}^{\bullet+}$, X1 = F7; X2 = F8; X3 = C9.

synthetic methodology to maximize the probability of preparing cycloadducts of RCN with IPs of less than ca. 13 eV by the step-by-step addition of RCN to an excess of sulfur homopolyatomic cations. This strategy proved to be successful, and $\mathbf{1CCl_3AsF_6}$ (IP[Cl_3CCN], 11.89 eV[10a]) was isolated in 77% yield. The recovered yields were lower if longer reaction times were used or the reagents were mixed directly. On the other hand, for the synthesis of F_5C_2CN, the kinetic reaction conditions were not important because of the relatively high IP of F_5C_2CN (13.4 eV[10b]), and the simultaneous mixing of the two reagents produced analytically pure product $\mathbf{1C_2F_5AsF_6}$ in 80% yield. Preliminary results of $S_4(AsF_6)_2/S_8(AsF_6)_2$ with other RCN of IPs lower than 13.5 eV (e.g., R = Cl, 12.4 eV; Br, 11.8 eV; I, 10.9 eV) show that they also successfully give $RCNSSSAsF_6$ salts.[9d] Thus, the generality of the preparations of $RCNSSSAsF_6$ by the reaction of RCN with a mixture of $S_n(AsF_6)_2$ (n = 4 and 8) has successfully been extended. Like $\mathbf{1CF_3AsF_6}$, the newly prepared salts $\mathbf{1CCl_3AsF_6}$ and $\mathbf{1C_2F_5AsF_6}$ are paramagnetic at room temperature with weak intercationic antiferromagnetic interactions in the solid state (see the Magnetic Properties of $\mathbf{1CCl_3AsF_6}$ and $\mathbf{1C_2F_5AsF_6}$ section).

Solid-State Structures of $\mathbf{1CCl_3AsF_6}$ and $\mathbf{1C_2F_5AsF_6}$. Experimental geometries of $\mathbf{1CCl_3}^{\bullet+}$ and $\mathbf{1C_2F_5}^{\bullet+}$ are shown in Figure 1. Their intracationic bond distances and angles are very similar to the calculated gas-phase geometries and those found for the related 7π radical cations $\mathbf{1CF_3}^{\bullet+}$ and **2** (Table 2). The AsF_6^- anions are of distorted O_h geometry (Figures S3 and S4 in the Supporting Information).

Each cation and anion of $\mathbf{1CCl_3AsF_6}$ is surrounded by eight counterions in an overall CsCl-type arrangement (Figure S1 in the Supporting Information). The majority of

(9) (a) Wood, D. J. Ph.D. Thesis, University of New Brunswick, Fredericton, Canada, 2001. (b) Cameron, T. S.; Decken, A.; Fang, M.; Parsons, S.; Passmore, J.; Wood, D. J. *J. Chem. Soc., Chem. Commun.* **1999**, 1801. (c) Cameron, T. S.; Decken, A.; Fang, M.; Passmore, J. *J. Chem. Soc., Chem. Commun.* **2001**, 1370. (d) Cameron, T. S.; Decken, A.; Kowalczyk, R. M.; McInnes, E. J. L.; Passmore, J.; Rawson, J. M.; Shuvaev, K. V.; Thompson, L. K. *J. Chem. Soc. Chem. Comm.* **2006**, in press.

(10) (a) Molder, U. H.; Pikver, R. J.; Koppel, I. A. Photoelectron spectra of molecules. 3. Nitriles. *Org. React.* (*Tartu*) **1983**, *20*, 230. (b) Calculated on the PBE1PBE/6-311+(2df) level of theory. The experimental IP of F_5C_2CN is unknown.

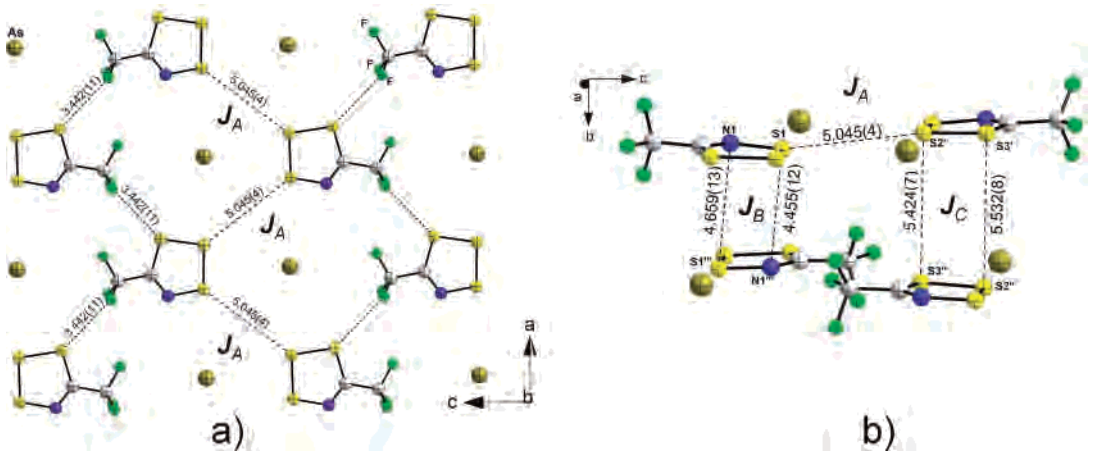

Figure 2. (a) Layer of cations and anions of $\mathbf{1CF_3AsF_6}$ in the *ac* plane. (b) Depiction of the packing of $\mathbf{1CF_3}^{\bullet+}$ along the *a* axis (only half of the unit cell shown in the *c* direction). Anions are designated by As for the sake of clarity.

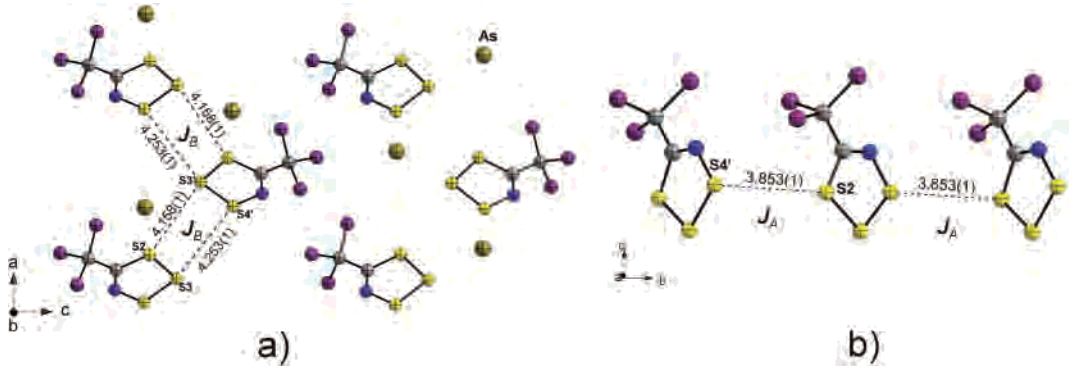

Figure 3. (a) Projection of half of the unit cell of $\mathbf{1CCl_3AsF_6}$ in the *b* direction onto the *ac* plane. Anions are designated by As for the sake of clarity. (b) Representative 1D chain of radical cations $\mathbf{1CCl_3}^{\bullet+}$ along the *b* axis.

the noncovalent S···F interactions are relatively long, consistent with the predominantly ionic nature of $\mathbf{1CCl_3AsF_6}$, as was also found for $\mathbf{1CF_3AsF_6}$ and **2**. However, the packing motif of $\mathbf{1CCl_3AsF_6}$ is markedly different from that in $\mathbf{1CF_3AsF_6}$, illustrating how relatively small changes in the substituent (in this case replacement of three F atoms by three Cl atoms) lead to drastic changes in the structure. The structure of $\mathbf{1CF_3AsF_6}$ contains alternating layers of cations and anions situated in the *ac* plane, in a NaCl-type arrangement.[6a] Monomeric radical cations $\mathbf{1CF_3}^{\bullet+}$ are linked by weak $CF_3^{\delta-}\cdots S^{\delta+}$ interactions into chains running along the *a* axis (Figure 2a). There are also interchain contacts at 5.045(4) Å between two S atoms, each belonging to the neighboring chains (the sum of the in-plane van der Waals radii of two S atoms, 3.20 Å[11]). This then may give a second chain of radicals linked via S···S interactions of 5.045(4) Å along the *a* axis. Additional chains result from interlayer interactions via two S···S [5.424(7) and 5.532(8) Å] and two S···N [4.455(12) and 4.659(13) Å] distances, as depicted in Figure 2b. In contrast, the radical cations $\mathbf{1CCl_3}^{\bullet+}$ produce shorter S···S contacts with a head-to-head- and tail-to-tail-like arrangement of radical cations (Figure 3), perhaps as a result of the lower electronegativity and larger size of the Cl atoms. When viewed along the *b* axis, the packing of $Cl_3CCNSSS^{\bullet+}$ can be described as 1D chains of radical cations connected by relatively short S2···S4′ interactions of 3.853(1) Å (the shortest intermolecular S···S distance in the structure; Figure 3b). In turn, the neighboring chains of $\mathbf{1CCl_3}^{\bullet+}$ are linked by means of S2···S3′ and S3···S4′ contacts [4.158(1) and 4.253(1) Å, respectively], as shown in Figure 3a.

In $\mathbf{1C_2F_5AsF_6}$, each cation and anion is surrounded by five anions and cations, respectively forming a square pyramid (Figure S2 in the Supporting Information). The arrangement of cations in $\mathbf{1C_2F_5AsF_6}$ bears a close resemblance to that in $\mathbf{1CCl_3AsF_6}$ in that they also arrange themselves in head-to-head and tail-to-tail fashion with respect to each other (Figure 4a). 1D chains of parallel (mean plane separation 3.2 Å; Figure 4b) radical cations are formed along the *b* axis albeit with a longer S3···S4′ distance of 4.266(4) Å [the nearest S···S contact in the $\mathbf{1CCl_3}^{\bullet+}$ chain is 3.853(1) Å]. The chains weakly interact via S3···S3′ contacts of 4.111-(8) Å in a pairwise manner, as shown in Figure 4. This motif is different from that seen in the structure of $\mathbf{1CCl_3AsF_6}$, where all of the interchain interactions between radical cations are equal and which can itself be viewed as a second chain (Figure 3a).

EPR Spectra of $\mathbf{1CCl_3AsF_6}$ and $\mathbf{1C_2F_5AsF_6}$. Solution EPR spectra of both $\mathbf{1CCl_3AsF_6}$ and $\mathbf{1C_2F_5AsF_6}$ in SO_2 consist of a single resonance with isotropic *g* values of

(11) Nyburg, S. C.; Faerman, C. H. *Acta Crystallogr., Sect. B* **1985**, *B41*, 274.

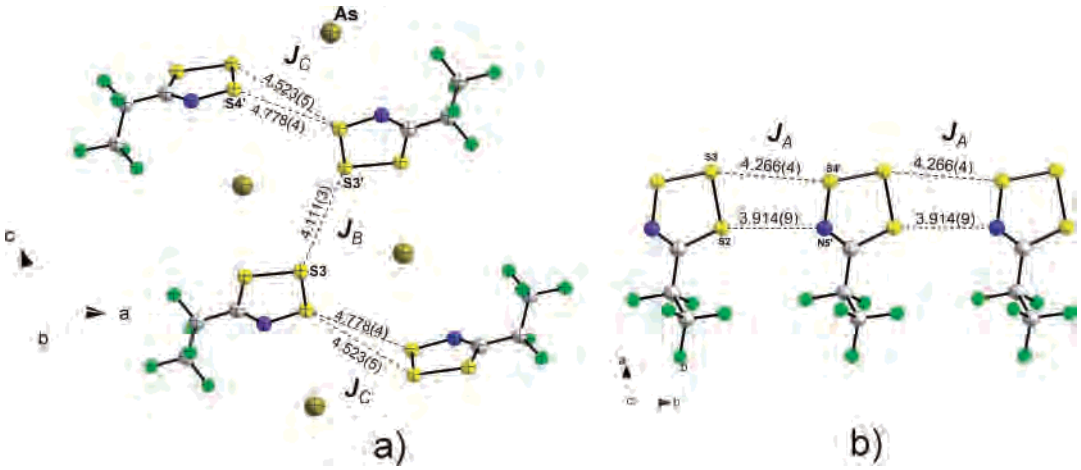

Figure 4. (a)Unit cell of $\mathbf{1C_2F_5AsF_6}$. Anions are designated by As for the sake of clarity. (b) Representative chain of radical cations $\mathbf{1C_2F_5}^{\bullet+}$ along the *b* axis.

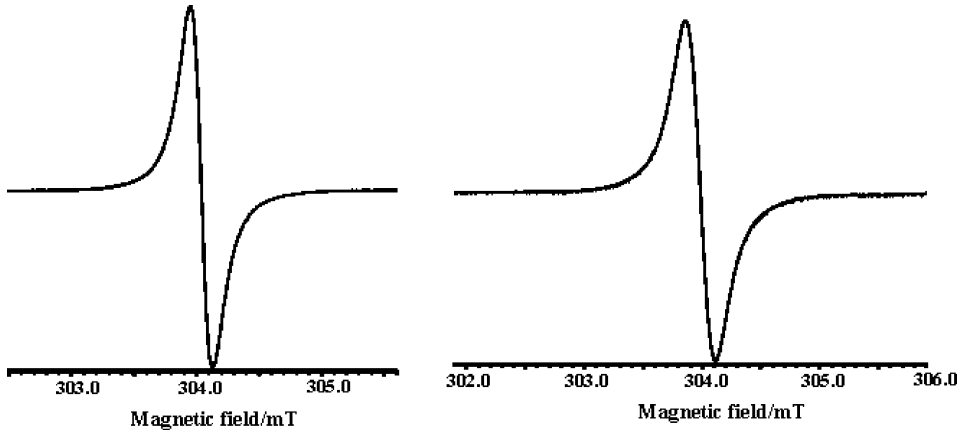

Figure 5. Isotropic EPR spectra of $\mathbf{1CCl_3AsF_6}$ (right) and $\mathbf{1C_2F_5AsF_6}$ (left) in SO_2 at −70 °C.

Table 3. Calculated [MPW1PW91/6-311+G(2df)] Spin Densities, Hyperfine Coupling Constants (*a*),[a] and NBO Charges of $\mathbf{1CF_3}^{\bullet+}$, $\mathbf{1CCl_3}^{\bullet+}$, and $\mathbf{1C_2F_5}^{\bullet+}$

	$1CF_3^{\bullet+}$			$1CCl_3^{\bullet+}$			$1C_2F_5^{\bullet+}$		
atom	spin density	*a*, G	NBO charge	spin density	*a*, G	NBO charge	spin density	*a*, G	NBO charge
C1	−0.00669	−1.73	−0.0161	−0.0167	−1.98	0.0119	−0.00800	−1.72	−0.00214
S2	0.277	3.70	0.3733	0.270	3.51	0.3566	0.283	3.81	0.3769
S3	0.355	4.20	0.2851	0.348	4.04	0.2746	0.356	4.20	0.2840
S4	0.339	4.30	0.5265	0.344	4.31	0.5276	0.335	4.24	0.5232
N5	0.0379	0.57	−0.2514	0.0481	0.82	−0.2536	0.0359	0.54	−0.2517
C6	−0.00469	−0.35	0.5623	0.00279	−0.33	−0.1232	−0.0052	−0.24	0.3427
F7	0.00141	1.0	−0.1555				0.0019	1.31	−0.1538
F8	−0.00132	1.0	−0.1686				−0.0012	−0.86	−0.1665
F9	0.00139	−0.45	−0.1555						
Cl1				0.00256	0.29	0.0729			
Cl2				−0.00211	−0.07	0.0604			
Cl3				0.00259	0.29	0.0729			
C9							0.00017	0.19	0.5464
F10							0.00030	0.11	−0.1671
F11							−0.000078	−0.013	−0.1742
F12							−0.00011	−0.009	−0.1578

[a] Calculated for ^{13}C, ^{33}S, ^{14}N, ^{19}F, and ^{35}Cl isotopes.

2.01675 and 2.01580, respectively (Figure 5). The larger *g* value for $\mathbf{1CCl_3}^{\bullet+}$ is due to the larger spin−orbit coupling constant of the Cl atoms compared to the F atoms in the C_2F_5 substituent group of $\mathbf{1C_2F_5}^{\bullet+}$. The spectra show no observable hyperfine coupling with N, Cl, or F. Previous EPR and theoretical studies performed on $\mathbf{1CF_3AsF_6}$[6a] and **2**[6c,9a] revealed a π^* singly occupied molecular orbital (SOMO) located predominantly on the S_3 fragment, with very little spin density found on the N atom and almost none on the CF_3 group (see Table 3). Results of calculations on the MPW1PW91/6-311+G(2df) level of theory presented in this paper for $\mathbf{1CF_3}^{\bullet+}$ are almost identical with those previously reported.[6a] Aside from the contributions to the *g* values, CF_3, CCl_3, and C_2F_5 groups do not appear to make any significant

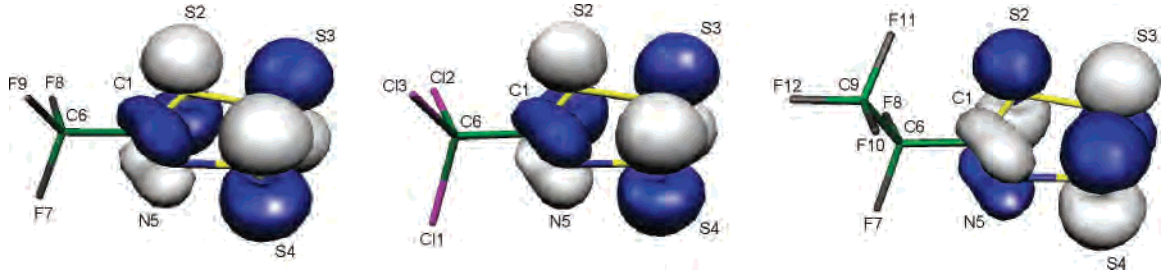

Figure 6. Calculated [MPW1PW91/6-311+G(2df)] SOMOs of $\mathbf{1CF_3}^{\bullet+}$, $\mathbf{1CCl_3}^{\bullet+}$, and $\mathbf{1C_2F_5}^{\bullet+}$.

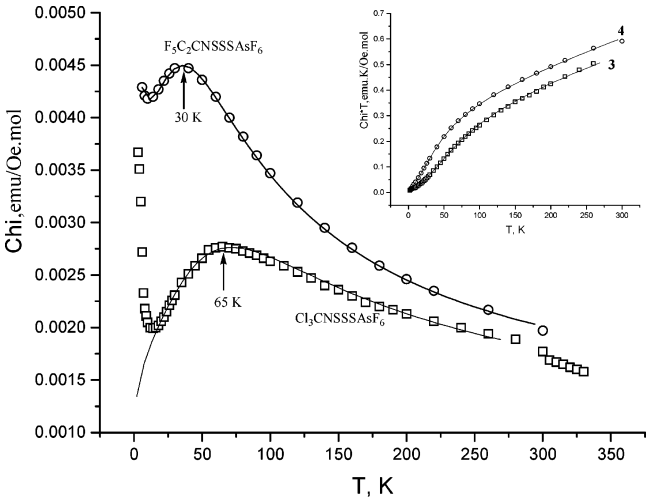

Figure 7. Temperature dependence of χ and χT (inset) of $\mathbf{1CCl_3AsF_6}$ (□) and $\mathbf{1C_2F_5AsF_6}$ (○). The solid lines indicate fits to a 1D Heisenberg $S = {}^1/_2$ chain. Fitting parameters are given in the text. Experimental data are given in Table S3 in the Supporting Information.

perturbations to the π^* SOMO (Figure 6), hence the similar nature of the EPR spectra and SOMOs of $\mathbf{1CF_3}^{\bullet+}$, $\mathbf{1CCl_3}^{\bullet+}$, and $\mathbf{1C_2F_5}^{\bullet+}$.

Conductivity of $\mathbf{1CCl_3AsF_6}$ and $\mathbf{1C_2F_5AsF_6}$. Pressed-pellet conductivity measurements performed on $\mathbf{1CCl_3AsF_6}$ and $\mathbf{1C_2F_5AsF_6}$ indicated Mott insulator behavior ($\sigma < 10^{-7}$ S/cm) in agreement with a lack of communication between unpaired electrons (see the Magnetic Properties of $\mathbf{1CCl_3AsF_6}$ and $\mathbf{1C_2F_5AsF_6}$ section). Weak overlap between π stacks combined with a very high on-site coulombic repulsion of ca. 22 eV (IP − EA[4e]) accounts for the low conductivities of $\mathbf{1CCl_3AsF_6}$ and $\mathbf{1C_2F_5AsF_6}$.

Magnetic Properties of $\mathbf{1CCl_3AsF_6}$ and $\mathbf{1C_2F_5AsF_6}$. The temperature-dependent values of χ for both $\mathbf{1CCl_3AsF_6}$ and $\mathbf{1C_2F_5AsF_6}$ were fitted by a 1D Heisenberg antiferromagnetic chain model[12] [$\mathbf{1CCl_3AsF_6}$, $J = -34$ cm^{-1}, $\theta = -9$ cm^{-1}, TIP = 0.00082, $\rho = 0.012$, $R(\chi) = 0.087$; $\mathbf{1C_2F_5AsF_6}$, $J = -21$ cm^{-1}, $\theta = -4.2$ cm^{-1}, TIP = 0.00092, $\rho = 0.065$, $R(\chi) = 0.003$], with magnetic moments of 2.02 and 2.17 μ_B per molecule at room temperature (Figure 7). The θ term was included in the fitting to account for the weaker coupling between the chains.

Magnetic interaction between organic radicals, including S,N radicals,[1h] has successfully been calculated using the density functional theory (DFT) formalism. This is performed by calculating the energy difference between the broken symmetry singlet and triplet states for an isolated radical pair with the same geometry as that in the X-ray. Using a similar approach, possible magnetic interactions for $\mathbf{1CCl_3AsF_6}$ and $\mathbf{1C_2F_5AsF_6}$ have been analyzed and summarized in Table 4 (the calculated J values quoted in the text are from B3LYP/6-31G* calculations). The strongest antiferromagnetic coupling between radical cations in $\mathbf{1CCl_3AsF_6}$ propagates along the b axis via an S···S interaction of 3.853(1) Å. A nonzero SOMO−SOMO overlap of an intrachain radical pair (see J_A in Figure 3b and A in Figure 8) produces a weak bonding interaction, thus stabilizing antiferromagnetic ground state. The calculated value of J_A (−52 cm^{-1}) within this radical pair is in good agreement with the experiment (−34 cm^{-1}). Another considerable magnetic interaction in the structure of $\mathbf{1CCl_3AsF_6}$ occurs within a secondary zigzag chain running along the a axis (J_B, Figure 3a). Despite notably long S···S linkages [4.158(1) and 4.253(1) Å], there is a relatively large bonding SOMO−SOMO overlap between the edges of each heterocyclic ring (B, Figure 8). We found that the calculated J_B value for an interchain radical pair B (−32 cm^{-1}) is only about half that of the primary chain, thus considerably deviating from the experimental θ interchain coupling constant (−9 cm^{-1}). This seems an odd result and may imply a higher degree of dimensionality present in the structure of $\mathbf{1CCl_3AsF_6}$, for which the 1D antiferromagnetic chain model is unable to account. Nonetheless, the latter model still gives a satisfactory fit of the experimental magnetic data of $\mathbf{1CCl_3AsF_6}$. This is not achieved by a 2D square-lattice model (see Figure S5 in the Supporting Information).

The values of χ for $\mathbf{1C_2F_5AsF_6}$ are larger than those for $\mathbf{1CCl_3AsF_6}$, consistent with smaller negative values of J and θ (Figure 7). The weaker interaction between radical cations $\mathbf{1C_2F_5AsF_6}$ is also reflected in its lower T_{max} (30 vs 65 K in $\mathbf{1CCl_3AsF_6}$). As in $\mathbf{1CCl_3AsF_6}$, the most significant magnetic interaction in $\mathbf{1C_2F_5AsF_6}$ propagates along the b axis with the molecules linked by S···S [4.266(4) Å] and S···N [3.914(9) Å] contacts (J_A, Figure 4b). The calculated intrachain coupling constant J_A (−20 cm^{-1}) was very close to the experimental value (−21 cm^{-1}). Secondary magnetic exchange pathways in the structure of $\mathbf{1C_2F_5AsF_6}$ include those via a set of long S···S contacts, as shown in Figure 4a (J_B and J_C). The magnitudes of these interchain interactions were calculated to be +0.066 cm^{-1} (J_B) and −4.0 cm^{-1} (J_C). These smaller values indicate that 1D magnetic chains in $\mathbf{1C_2F_5AsF_6}$ are well isolated from each other, in contrast to the structure of $\mathbf{1CCl_3AsF_6}$. This also explains the much better agreement

(12) Bonner, J. C.; Fischer, M. E. *Phys. Rev.* **1964**, *135*, A640.

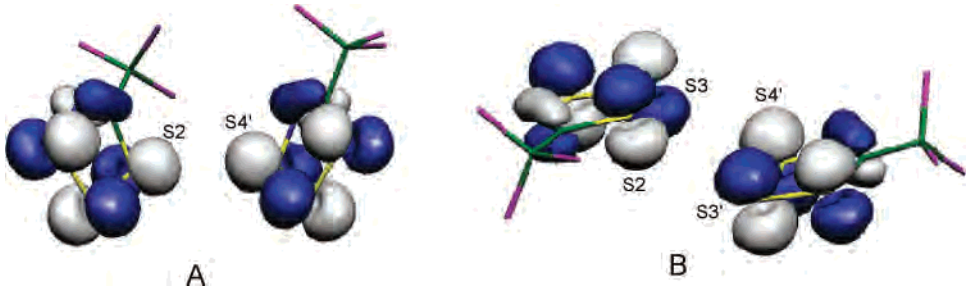

Figure 8. Illustration of bonding (antiferromagnetic) for intrachain (A) and interchain (B) overlap between SOMOs of radical pairs **1CCl$_3$AsF$_6$**.

Table 4. Compilation of Nearest Intermolecular S···S and S···N Contacts and the Corresponding Calculated Coupling Constants of **1CF$_3$AsF$_6$**, **1CCl$_3$AsF$_6$**, and **1C$_2$F$_5$AsF$_6$**

			J_{calcd}, cm^{-1}			
pathway	contact	d, Å	B3LYP/6-31g*	MPW1PW91/6-31g*	PBE1PBE/6-31g*	J_{exptl}, cm^{-1}
			1CF$_3$AsF$_6$			
J_A	S1···S2′	5.045(4)	−0.15	−0.11	−0.11	
J_B	S1···N1‴	4.659(13)	−1.29	−1.0	−1.0	
	S1‴···N1	4.455(12)				
J_C	S2′···S3″	5.532(8)	−0.70	−0.48	−0.48	
	S3′···S2″	5.424(7)				
			1CCl$_3$AsF$_6$			
J_A	S2···S4′	3.853(1)	−52	−42	−44	−34
J_B	S2···S3′	4.158(1)	−32	−26	−27	−9
	S3···S4′	4.253(1)				
			1C$_2$F$_5$AsF$_6$			
J_A	S2···N5′	3.914(9)	−20	−15	−16	−21
	S3···S4′	4.266(4)				
J_B	S3···S3′	4.111(8)	+0.066	+0.22	+0.29	
J_C	S3···S4″	4.523(6)	−4.0	−3.0	−3.1	−4.2
	S4···S4″	4.778(5)				

between experimental and calculated J constants in the structure of **1C$_2$F$_5$AsF$_6$**. Surprisingly, the longer S···S separation produces an exchange coupling 2 orders larger in magnitude than that of the shorter S···S distance. The striking difference can be attributed to the poor SOMO−SOMO overlap for radical pair B, as compared to that of C (Figure 9). Therefore, on the basis of DFT calculations, we can relate J_A and J_C coupling constants to the experimental values J and θ, respectively. This example highlights the importance of consideration of orbital directionality in the magnetic interaction between radical centers and the utility of DFT calculations in the analysis of such magnetic exchange pathways.

Previously, **1CF$_3$AsF$_6$** was shown to be an almost perfect paramagnet, obeying the Curie−Weiss law down to about 5 K with $\theta = -5.8$ K.[6a,13] The data can be more rigorously fit by the alternating chain model ($J = -7.46$ K; $\alpha = 0.563$), most likely as a result of undergoing a spin−Peierls transition at very low temperature.[13] The structure of **1CF$_3$AsF$_6$** also contains chains of radical cations linked by long S···S contacts of 5.045(4) Å (J_A, Figure 2a).[6a] There are, however, two additional significant magnetic interactions arising from a set of interlayer S···S and S···N distances (J_B and J_C, Figure 2b). In the present paper, we have carried out DFT calculations for each local magnetic coupling with the magnetic pathways as illustrated in Figure 2. All $|J|$ values were found to be <1 cm^{-1}, consistent with a very weak communication between unpaired electrons. Within the mean-field approximation,[14] the Weiss constant can be calculated as the double sum of all J terms, leading to −6.16 K, in excellent agreement with the experimental value ($\theta = -5.8$ K).

Chart 2

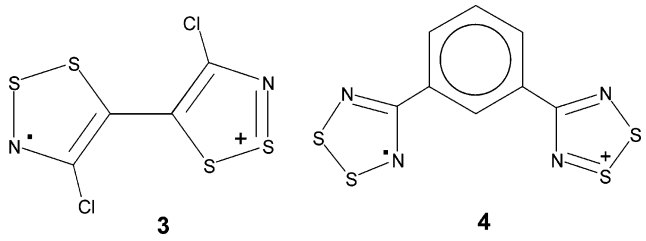

Other examples of S,N radical cations to produce ladder-types arrays, akin to **1CCl$_3$AsF$_6$** and **1C$_2$F$_5$AsF$_6$**, have previously been described by Oakley and co-workers in the structures of **3**[15a] and **4**[15b] (Chart 2). In the solid state, both compounds contain uniform 1D chains albeit with much stronger intrachain J coupling constants of −170 cm^{-1} (**3**)[15c] and −465 cm^{-1} (**4**), respectively.

Our EPR and theoretical studies show that the unpaired spin densities in **1CF$_3$**$^{\bullet+}$, **1CCl$_3$**$^{\bullet+}$, and **1C$_2$F$_5$**$^{\bullet+}$ are almost entirely localized on the CNSSS$^{\bullet+}$ moiety (Figure 6 and

(13) Antorrena, G. P. Ph.D. Thesis, Universidad de Zaragoza, Zaragoza, Spain, 1998.

(14) Kahn, O. *Molecular magnetism*; VCH: New York, 1993.

(15) (a) Barclay, T. M.; Beer, L.; Cordes, A. W.; Haddon, R. C.; Itkis, M. E.; Oakley, R. T.; Preuss, K. E.; Reed, R. W. *J. Am. Chem. Soc.* **1999**, *121*, 6657. (b) Britten, J. F.; Cordes, A. W.; Haddon, R. C.; Itkis, M. E.; Oakley, R. T.; Reed, R. W.; Robertson, C. M. *CrystEngComm* **2002**, *4*, 205. (c) The value was obtained from our fit to the 1D antiferromagnetic chain using experimental data kindly provided by R. T. Oakley.

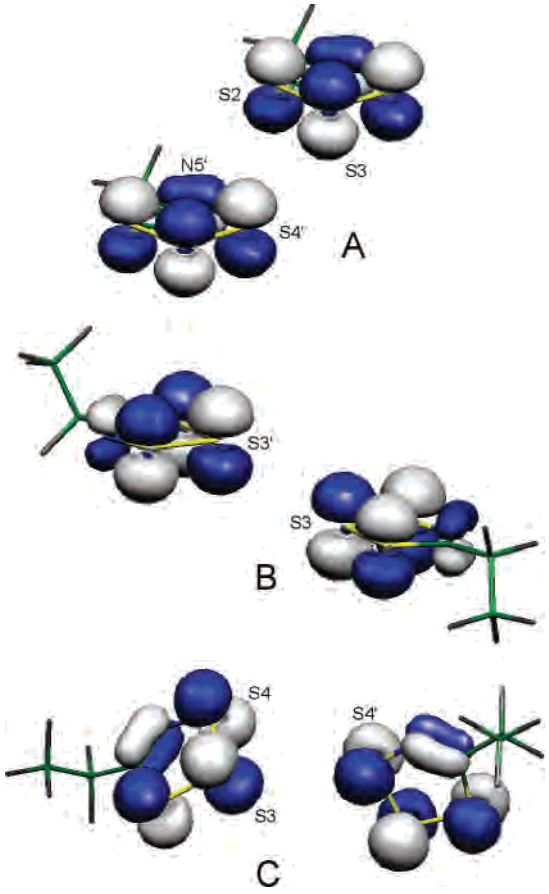

Figure 9. Illustration of SOMO−SOMO overlap for one intrachain (A) and two interchain (B and C) radical pairs in the structure of $\mathbf{1C_2F_5AsF_6}$.

Table 3); i.e., there is a negligible substituent effect on the electronic properties of the heterocyclic ring, with a non-significant change in the nature of SOMO. Therefore, different magnetic properties of $\mathbf{1CF_3AsF_6}$, $\mathbf{1CCl_3AsF_6}$, and $\mathbf{1C_2F_5AsF_6}$ arise from different packing motifs and not the electronic nature of the substituent. This is very similar to the well-known related $RCNSSN^{\bullet}$ system,[1] investigated by Rawson et al. in a systematic theoretical and experimental study showing the packing motifs to be the major factor in determining the sign and magnitude of magnetic exchange interaction.[1g,h] In both $RCNSSS^{\bullet+}$ and $RCNSSN^{\bullet+}$ radicals, anisotropic S atoms bear significant spin densities, and their interradical arrangements determine their magnetic properties. This situation contrasts with that in nitronyl nitroxide radicals, in the structures of which no clear correlation between geometrical arrangements of N−O moieties (bearing most of the spin densities) and the magnetic properties is observed, and the substituent groups possessing very small spin densities often play a crucial role in mediating the magnetic coupling between radical centers.[16]

Conclusion

In the present paper, we have established the potential of preparing a large class of 7π $RCNSSS^{\bullet+}$ radical cations and a relationship between the geometry of the interradical S··· ·S interaction and the strength of the magnetic coupling. We have demonstrated the utility of DFT calculations in the analysis and assignment of possible magnetic exchange pathways in the structures of $RCNSSS^{\bullet+}$ ring systems. This will aid in the understanding of the more complex physical and magnetic behavior of **2**, the *paramagnetic liquids*, e.g., $F_3CCSNSCCF_3$[2f] and $F_3CCNSSN$,[2d] as well as in the design and synthesis of other derivatives of **1** with unusual properties.

Acknowledgment. We are grateful to NSERC for providing funding (to J.P., K.V.S., L.K.T., and S.M.M.), J. M. Rawson for assisting with the fitting of magnetic data and use of his program *MAGNET*, R. T. Oakley for carrying out pressed-pellet conductivity measurements, and F. Palacio and G. P. Antorrena for allowing us to quote results from a Ph.D. thesis.[13]

Supporting Information Available: Crystallographic data in CIF format, figures illustrating various diagrams of $\mathbf{1CCl_3AsF_6}$ and $\mathbf{1C_2F_5AsF_6}$, and tables of various values for $\mathbf{1CCl_3AsF_6}$ and $\mathbf{1C_2F_5AsF_6}$. This material is available free of charge via the Internet at http://pubs.acs.org.

IC050577N

(16) Novoa, J. J.; Deumal, M. *Struct. Bonding* **2001**, *100*, 33.